



Optics Letters

Experimental demonstration of spatial rogue waves in the passively Q-switched Nd:YAG laser

ROZA NAVITSKAYA,^{1,2}  IHAR STASHKEVICH,¹ STANISLAV DEREVYANKO,²  AND ALINA KARABCHEVSKY^{2,*} 

¹Faculty of Physics, Belarusian State University, 4 Nezalezhnasti Avenue, 220030 Minsk, Belarus

²School of Electrical and Computer Engineering, Ben Gurion University of the Negev, Beer Sheva, Israel

*Corresponding author: alinak@bgu.ac.il

Received 29 April 2021; revised 20 June 2021; accepted 6 July 2021; posted 7 July 2021 (Doc. ID 430141); published 30 July 2021

The generation of spatial rogue waves, or “hot spots,” is demonstrated experimentally in the passively Q-switched Nd:YAG laser system operating in a low-power regime well below the self-focusing limit. Here, we report the dependence of rogue wave statistics on the number of transverse modes that interact in the laser cavity. Our observations show that spatial rogue waves are most likely to occur when the laser exhibits complex output beam configurations that are formed by a large number of interacting high-order transverse modes. These results confirm the hypothesis that one of the main factors affecting the emergence of spatial rogue waves in solid-state lasers is the number of laser transverse modes. © 2021 Optical Society of America

<https://doi.org/10.1364/OL.430141>

The emergence, dynamics, and prediction of rogue waves (RWs), also referred to as freak waves or extreme events, has been the focus of interest in diverse fields of science over the last 15 years. The traditional notion of RWs is related to rare events of large amplitude that appear unpredictably on the ocean surface and disappear without a trace. In 2007, in the pioneering paper, Solli *et al.* [1] proposed an analogy between the RWs in optics and hydrodynamics and thus started a new sub-field in optics. Since then, RWs have been investigated in different optical systems including integrable systems, such as fibers or waveguides with dispersion and nonlinearity [2–6], and dissipative systems, mostly presented by different types of lasers. Thus, RWs have been observed in mode-locked fiber lasers [7–12], Kerr-lens mode-locked Ti:sapphire lasers [13], all-solid-state lasers passively Q-switched by the use of a saturable absorber [14–16], lasers with modulation of losses [17–19], free-running lasers [19], vertical-cavity surface-emitting lasers [20,21], and semiconductor lasers [22]. The recent developments of optical RW investigation are summarized in several review papers [23–25].

Historically, investigations were mostly focused on the study of temporal RWs that represent pulses with extremely high intensities relative to the typical intensities in a pulse time train. Temporal RWs can be observed at the output of mode-locked and passively Q-switched lasers operating in non-stationary or chaotic regimes (see, e.g., [16]). However, in recent years, the study of spatial and spatiotemporal RWs has gathered much

attention. The spatiotemporal dynamics of optical pulses have been demonstrated in multimode fibers (formation of solitons [26], spatiotemporal instability [27], beam self-cleaning [28]), and mode-locked fiber lasers (spatiotemporal mode-locking [29] and multiple-soliton [30], to name just a few).

Yet there exists a purely spatial (and also spatiotemporal) manifestation of the RW phenomenon known as “hot spots” that correspond to tightly focused spots in the transverse cross section of the beam with peak intensities much higher than the average beam intensity. This phenomenon has been known in laser physics for many years—long before the discovery of RWs in optical fiber geometry [31]. It was observed that in high-power lasers, the optical elements or the laser crystal itself can be damaged by spontaneously created hot spots with extremely high intensities [31,32]. It was conjectured that such hot spots emerge due to the spontaneous coupling of transverse and/or longitudinal laser modes, which then leads to further breakup of the laser beam under nonlinear effects of filamentation and catastrophic self-focusing (in Kerr media), which are especially pronounced in high-power lasers [31,33,34].

However, despite years of research, the main factors thought to be affecting the emergence of the hot spots remain elusive. For example, it is a well-established fact now that nonlinearity is not strictly necessary to observe the enhanced probability of occurrence of a RW, and the heavy-tail statistics of wave intensity distribution have been reported in purely linear systems [35,36]. Rather, it is the complex interaction of a large number of cavity modes that leads to the enhanced probability of hot spot emergence. While the role of transverse effects in the dynamics and statistics of Q-switched cavity lasers was discussed in several publications [14–16,21,37], these papers concentrated almost exclusively on time-resolved spatiotemporal dynamics.

In this work, we do not focus on the correlation between the emergence of temporal and spatial RWs but directly investigate the influence of the laser transverse mode configuration on the formation of hot spots, which we associate with spatial RWs. We argue that in the low-power regime of laser operation, well below the self-focusing limit, there is a direct relation between the total number of transverse lasing modes, the index (transverse wavenumber) of the lasing mode, and the emergent spatial field distributions. We argue that it is the combination of the high

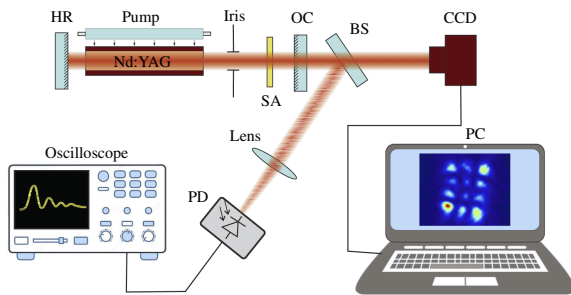


Fig. 1. Scheme of the experimental setup. Main elements shown are: Nd:YAG, laser active element with lamp pumping; HR, highly reflective mirror; OC, output coupler; SA, saturable absorber; BS, beam splitter; CCD, camera registering the transverse profile of the laser beam; PC, computer with software to control the camera; PD, photodiode; oscilloscope displaying the temporal intensity profile of the Q -switched pulse.

total number of lasing modes and the high order of the lasing mode that brings about the emergence of the spatial RWs.

We have implemented a simple and robust scheme for experimentally controlling the number and order of the lasing modes and observing both the spatial patterns and statistics of the cavity field. Our experimental setup represents a passively Q -switched Nd:YAG laser (see Fig. 1).

The Nd:YAG laser with flashlamp pumping operates in a pulsed regime with a 5 Hz repetition rate. The cavity length is 70 cm, and the length of the laser crystal is 10 cm. The output mirror has a reflection coefficient of 63% and a flat surface, and the HR mirror is spherical with radius of curvature equal to 360 cm. Passive Q -switching is realized with the use of a LiF crystal containing F_2^- color centers. The initial transmittance of this saturable absorber is 31%. The pump energy is 13 J, while the threshold energy required for lasing in Q -switch mode is 10.5 J. Typical Q -switched pulse energy and duration are about 3 mJ and 20 ns corresponding to the power in the cavity of 0.41 MW, which is much less than the minimal power required for self-focusing in Nd:YAG (5.3 MW) [33]. Thus, the laser operates in a low-power regime well below the self-focusing limit with the main source of nonlinearity being not the Kerr effect, but rather saturable absorption in the passive Q -switch shutter. However, the impact of Kerr effects cannot be fully discarded since it was shown in [28] that it can affect the beam propagation even for sub-critical powers (at least in optical fibers). The output beam spatial profile is recorded by a camera synchronized with the laser repetition rate (200 ms exposition) so that it captures the transverse intensity distribution integrated over the duration of the Q -switched pulse. To record the output

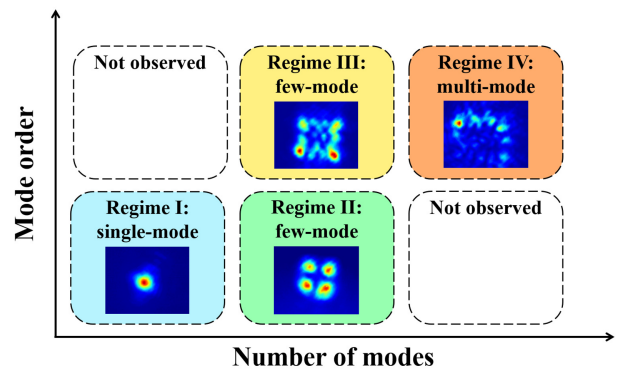


Fig. 2. Laser mode configurations investigated in the experiment.

pulse temporal profile, a photodiode connected to a digital oscilloscope was used. However, it was not synchronized with the camera and was employed only to ensure that the laser was in Q -switched mode.

To investigate the connection between the number of transverse modes that participate in the laser generation and characteristics of spatial RWs emerging at the laser output, we analyzed the pulse-to-pulse transverse intensity distributions captured by the camera, and calculated the RW statistics for four different mode configurations. These configurations and the corresponding laser generation regimes are summarized in Table 1 and shown schematically in Fig. 2.

The described beam configurations were obtained by tuning the iris diaphragm size and the laser mirrors alignment. Specifically, the diaphragm size was changed to vary the number of lasing modes and their orders (lower-order modes with smaller values of the transverse wavenumber were obtained for smaller diaphragm sizes, higher-order modes for larger diaphragm sizes), while tuning the laser mirrors was used to change the mode-dependent losses and thus obtain different output beam patterns. Here we note that both the iris size and alignment of the laser mirrors had to be changed to get all the observed generation regimes. By tuning only one of these parameters, for example, the iris size for the fixed mirrors alignment, it was not possible to get all the regimes below.

The pulse-to-pulse beam profiles were characterized in terms of peak intensity over the transverse distribution. The statistical distribution of the peak intensity values recorded for a large number of camera shots corresponding to different Q -switched pulses was used to study the probability of RW generation. Figure 3 illustrates the obtained pulse-to-pulse peak intensity

Table 1. Four Laser Mode Configurations and Corresponding Generation Regimes Investigated in the Experiment^a

Regime	Number of Modes	Mode Order (max)	Output Beam Configuration
I	Single-mode (1)	Low-order (LG ₀₀)	Lasing at a fundamental transverse mode
II	Few-mode (2–4)	Low-order (HG ₂₁)	Each Q -switched pulse corresponds to a certain mode with small influence of the other modes
III	Few-mode (2–4)	High-order (HG ₃₂ , HG ₂₃)	Each Q -switched pulse corresponds to a certain mode with small influence of the other modes
IV	Multi-mode (>4)	High-order (LG ₀₁₁)	The output beam patterns are complex, showing the contribution of several transverse modes

^aTypical values of the number of lasing modes and index of the highest-order mode observed in regimes I–IV are indicated in brackets.

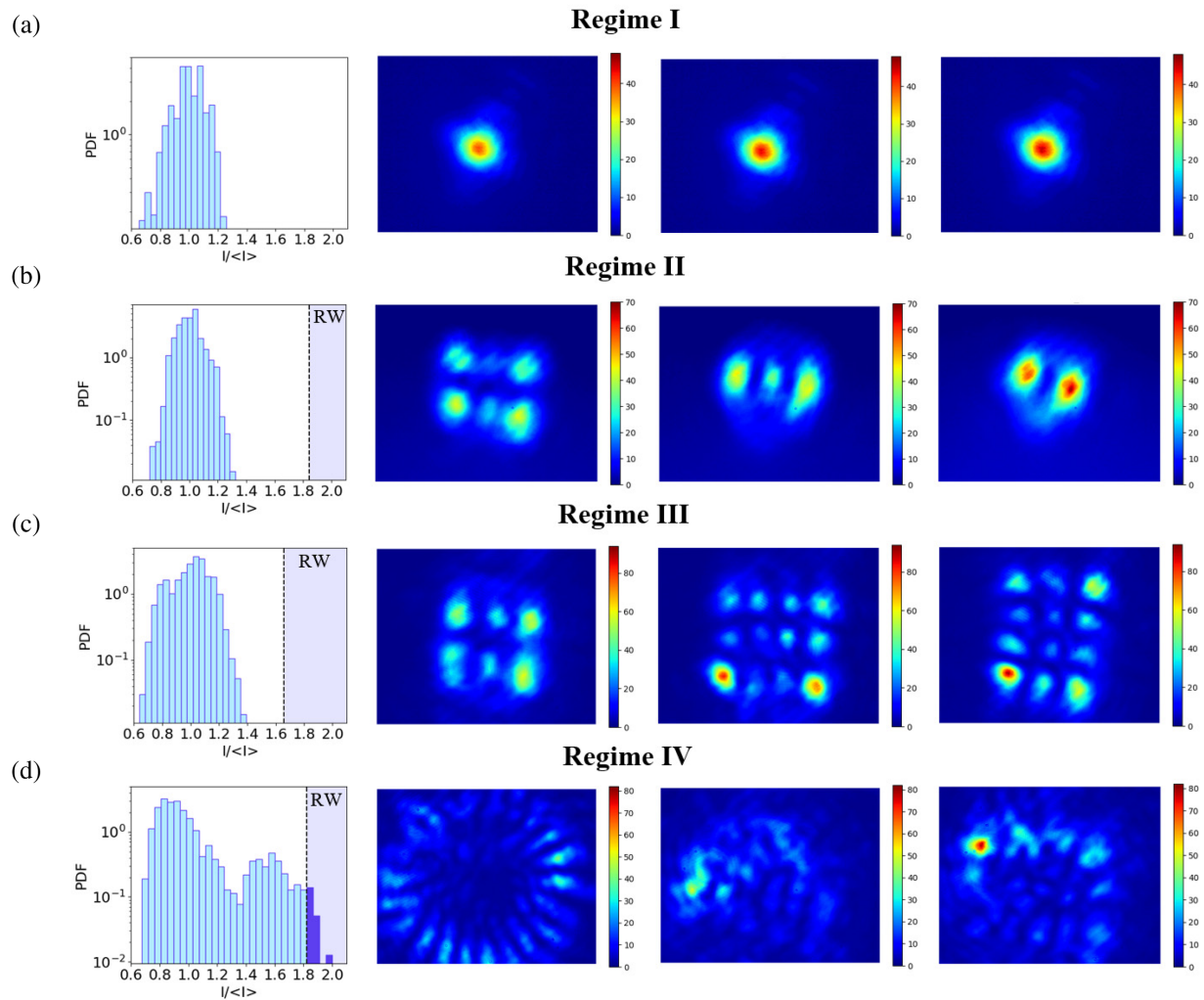


Fig. 3. Statistics of pulse-to-pulse peak intensity over the transverse intensity profile and example profiles for different laser mode configurations described in Table 1. The intensity distributions (in a.u.) in each row have common scaling. The dashed lines indicate the RW limits calculated in Fig. 4. In (a), the RW limit ($= 2.73$) is not shown, as it exceeds the common axis range.

statistics and provides examples of the transverse intensity distributions with (a)–(d) displaying typical mode configurations corresponding to regimes I–IV, respectively.

The observed pulse-to-pulse peak intensity relative to the average value varied in the range from 0.7 to 1.3 for cases (a) and (b) (regimes I and II) when there was only one main lasing mode [which can be different for different Q -switched pulses in (b)]. These cases exhibit no evident spatial RWs. The tendency to hot spot formation is noticed in (c) (regime III), when higher-order modes are involved in the generation. Although the beam patterns correspond mainly to certain Hermite–Gaussian modes (HG₂₁, HG₃₂, and HG₂₃ from left to right), it is seen that there is still some influence of the other modes. This results in such beam configurations where the energy is focused mainly in one of the mode lobes. However, the variations in peak intensity are not larger than 1.7 of the average value. Finally, case (d) (regime IV) shows clear evidence of hot spots formation. Here, the interaction of several higher-order lasing modes results in various and complex intensity distributions. The output beam profiles can be either close to a certain high-order mode (e.g., LG₀₁₁, left), represent superposition of several modes without extremely

focused spots (center), or represent a superposition of modes resulting in a spatial RW (right). This spatial RW corresponds to a small focused spot with peak intensity almost twice as large as the average value of the pulse-to-pulse peak intensities. The peak intensity statistics in (d) have two pronounced peaks. The first of them corresponds to the distribution of the “ordinary” beam patterns without hot spots, and the second one we attribute to the generation of spatial RWs.

In addition to the pulse-to-pulse statistics of the peak intensity, intensity statistics over 2D transverse beam profiles are analyzed as well to determine whether the observed hot spots are indeed spatial RWs. For this, the beam intensities were compared with the significant wave height (SWH), which represents a commonly used parameter to characterize RWs. The SWH was calculated as the average of the highest one-third of amplitudes, and the RW limit for intensities was considered to be $(2 \times SWH)^2$. Figure 4 shows the probability density functions (PDFs) calculated over a different number (3–32) of 2D transverse intensity distributions for each of the laser generation regimes I–IV. The shaded areas in Figs. 3 and 4 indicate RW regions with the limits calculated independently

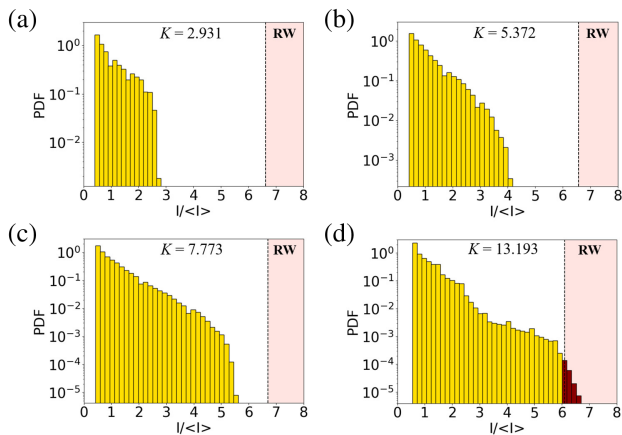


Fig. 4. 2D intensity statistics calculated over a number of transverse beam profiles for (a) regime I, (b) regime II, (c) regime III, and (d) regime IV. Also shown are the values of the kurtosis K .

for regimes I–IV. Background values (intensity < 7 a.u.) are discarded from the statistics. Thus, it is seen that spatial RWs are present only in regime IV [Figs. 4(d) and 3(d)] and are associated with those beam patterns that have the largest peak intensities, such as the rightmost one in Fig. 3(d). The PDF in this case has a pronounced L-shaped form, which is another criterion of RW formation. The long tails of the PDFs are commonly quantified by kurtosis K , defined as the ratio of the fourth and squared second moments. While regime I, shown in Fig. 4(a), corresponds to K close to three, the value of kurtosis for regime IV [Fig. 4(d)] is larger than 13, thus supplementing the observed L-shaped form of the PDF. These arguments confirm that the hot spots observed in specific beam profiles in regime IV are indeed spatial RWs.

To conclude, we obtained experimentally the generation of spatial RWs in the passively Q -switched Nd:YAG laser operating in the low-power regime and investigated the probability of the spatial RW formation for different laser mode configurations. We demonstrated that spatial RWs emerge only in the case of complex laser beam profiles, formed by a large number of high-order transverse modes nonlinearly interacting in the cavity. These results support the hypothesis that one of the most probable mechanisms of spatial RW formation in lasers is the nonlinear interaction of transverse modes. However, the exact role of nonlinearity as well the relationship between spatial and temporal RWs still requires further investigation and is left for future study.

Funding. Belarusian Republican Foundation for Fundamental Research (F21IZR-005); Israel Science Foundation (2598/20).

Disclosures. The authors declare no conflicts of interest.

Data Availability. Data underlying the results presented in this paper are not publicly available at this time but may be obtained from the authors upon reasonable request.

REFERENCES

- D. R. Solli, C. Ropers, P. Koonath, and B. Jalali, *Nature* **450**, 1054 (2007).
- J. M. Dudley, F. Dias, M. Erkintalo, and G. Genty, *Nat. Photonics* **8**, 755 (2014).
- B. Kibler, J. Fatome, C. Finot, G. Millot, F. Dias, G. Genty, N. Akhmediev, and J. M. Dudley, *Nat. Phys.* **6**, 790 (2010).
- M. Narhi, B. Wetzel, C. Billet, S. Toenger, T. Sylvestre, J. Merolla, R. Morandotti, F. Dias, G. Genty, and J. Dudley, *Nat. Commun.* **7**, 13675 (2016).
- P. Walczak, S. Randoux, and P. Suret, *Phys. Rev. Lett.* **114**, 143903 (2015).
- D. S. Agafontsev and V. E. Zakharov, *Nonlinearity* **28**, 2791 (2015).
- J. M. Soto-Crespo, P. Grelu, and N. Akhmediev, *Phys. Rev. E* **84**, 016604 (2011).
- C. Lecaplain, P. Grelu, J. M. Soto-Crespo, and N. Akhmediev, *J. Opt.* **15**, 064005 (2013).
- A. F. J. Runge, C. Aguerarary, N. G. R. Broderick, and M. Erkintalo, *Opt. Lett.* **39**, 319 (2014).
- M. Liu, A. P. Luo, W.-C. Xu, and Z. C. Luo, *Opt. Lett.* **41**, 3912 (2016).
- L. Gao, L. Kong, Y. Cao, S. Wabnitz, H. Ran, Y. Li, W. Huang, L. Huang, M. Liu, and T. Zhu, *Opt. Express* **27**, 23830 (2019).
- D. V. Churkin, S. Sugavanam, N. Tarasov, S. Khorev, S. V. Smirnov, S. M. Kobtsev, and S. K. Turitsyn, *Nat. Commun.* **6**, 7004 (2015).
- M. G. Kovalsky, A. A. Hnilo, and J. R. Tredicce, *Opt. Lett.* **36**, 4449 (2011).
- C. Bonazzola, A. Hnilo, M. Kovalsky, and J. Tredicce, *J. Opt.* **15**, 064004 (2013).
- C. R. Bonazzola, A. A. Hnilo, M. G. Kovalsky, and J. R. Tredicce, *Phys. Rev. A* **92**, 053816 (2015).
- C. Bonazzola, A. Hnilo, M. Kovalsky, and J. Tredicce, *Phys. Rev. E* **97**, 032215 (2018).
- N. Granese, A. Lacapmesure, M. Agüero, M. Kovalsky, A. Hnilo, and J. Tredicce, *Opt. Lett.* **41**, 3010 (2016).
- C. Metayer, A. Serres, E. Rosero, W. A. S. Barbosa, F. M. de Aguiar, J. R. R. Leite, and J. R. Tredicce, *Opt. Express* **22**, 19850 (2014).
- M. Nie, Y. Jiang, X. Fu, and Q. Liu, *IEEE J. Quantum Electron.* **56**, 1700205 (2020).
- C. Riboldi, S. Barland, F. Prati, and G. Tissoni, *Phys. Rev. A* **95**, 023841 (2017).
- S. Coulibaly, M. G. Clerc, F. Selmi, and S. Barbay, *Phys. Rev. A* **95**, 023816 (2017).
- J. Ahuja, D. B. Nalawade, J. Zamora-Munt, R. Vilaseca, and C. Masoller, *Opt. Express* **22**, 28377 (2014).
- N. Akhmediev, B. Kibler, F. Baronio, M. Belić, W. Zhong, Y. Zhang, W. Chang, J. Soto-Crespo, P. Vouzas, P. Grelu, C. Lecaplain, K. Hammani, S. Rica, A. Picozzi, M. Tliidi, K. Panajotov, A. Mussot, A. Bendahmane, P. Szriftgiser, G. Genty, J. Dudley, A. Kudlinski, A. Demircan, U. Morgner, S. Amiraranashvili, C. Brée, G. Steinmeyer, C. Masoller, N. Broderick, A. Runge, M. Erkintalo, S. Residori, U. Bortolozzo, F. Arecchi, S. Wabnitz, C. Tiofack, S. Coulibaly, and M. Taki, *J. Opt.* **18**, 063001 (2016).
- J. M. Dudley, G. Genty, A. Mussot, A. Chabchoub, and F. Dias, *Nat. Rev. Phys.* **1**, 675 (2019).
- Y. Song, Z. Wang, C. Wang, K. Panajotov, and H. Zhang, *Adv. Photon.* **2**, 024001 (2020).
- W. H. Renninger and F. W. Wise, *Nat. Commun.* **4**, 1719 (2013).
- U. Tegin and B. Ortac, *IEEE Photon. Technol. Lett.* **29**, 2195 (2017).
- K. Krupa, A. Tonello, B. M. Shalaby, M. Fabert, A. Barthélémy, G. Millot, S. Wabnitz, and V. Couderc, *Nat. Photonics* **11**, 237 (2017).
- L. G. Wright, D. N. Christodoulides, and F. W. Wise, *Science* **358**, 94 (2017).
- Y. Ding, X. Xiao, P. Wang, and C. Yang, *Opt. Express* **27**, 11435 (2019).
- G. Arisholm, in *OSA TOPS, Advanced Solid State Lasers* (Optical Society of America, 1997), Vol. **10**, p. 109.
- W. Koechner, in *Solid-State Laser Engineering* (Springer, 2006), pp. 680–701.
- W. Koechner, in *Solid-State Laser Engineering* (Springer, 2006), pp. 156–207.
- H. Bercegol, P. Bouchut, L. Lamaignère, B. L. Garrec, and G. Razé, *Proc. SPIE* **5273**, 312 (2004).
- A. Mathis, L. Froehy, S. Toenger, F. Dias, G. Genty, and J. M. Dudley, *Sci. Rep.* **5**, 12822 (2015).
- C. Liu, R. E. C. van der Wel, N. Rotenberg, L. Kuipers, T. F. Krauss, A. D. Falco, and A. Fratalocchi, *Nat. Phys.* **11**, 358 (2015).
- J. Dong and K. Ueda, *Phys. Rev. A* **73**, 053824 (2006).